

See discussions, stats, and author profiles for this publication at: <https://www.researchgate.net/publication/333485914>

# Exploring coarse- to fine-scale approaches for mapping and estimating forest volume from Brazilian National Forest Inventory data

Article in *Forestry* · May 2019

DOI: 10.1093/forestry/cpz030

CITATIONS

2

READS

192

9 authors, including:



**Hassan Camil David**

Brazilian Forest Service

39 PUBLICATIONS 162 CITATIONS

[SEE PROFILE](#)



**David W. MacFarlane**

Michigan State University

60 PUBLICATIONS 1,052 CITATIONS

[SEE PROFILE](#)



**Sylvio Péllico Netto**

Universidade Federal do Paraná

165 PUBLICATIONS 785 CITATIONS

[SEE PROFILE](#)



**Ana Paula Dalla Corte**

Universidade Federal do Paraná

303 PUBLICATIONS 1,136 CITATIONS

[SEE PROFILE](#)

Some of the authors of this publication are also working on these related projects:



Métodos para análise, classificação e monitoramento das Paisagens Rurais Brasileiras no âmbito do Inventário Florestal Nacional do Brasil (IFN-BR) [View project](#)



Studying the architecture of urban trees using terrestrial laser scanners. [View project](#)

## Exploring coarse- to fine-scale approaches for mapping and estimating forest volume from Brazilian National Forest Inventory data

Hassan C. David<sup>1\*</sup>, David W. MacFarlane<sup>2</sup>, Sylvio Péllico Netto<sup>3</sup>, Ana Paula Dalla Corte<sup>3</sup>, Daniel Piotto<sup>4</sup>, Yeda M. M. de Oliveira<sup>5</sup>, Vinicius A. Morais<sup>6</sup>, Carlos R. Sanquetta<sup>3</sup> and Rorai P. M. Neto<sup>7</sup>

<sup>1</sup>Departament of Forestry, Rural Federal University of Amazonia, Presidente Tancredo Neves Avenue, n. 2501 Belém, PA, Brazil

<sup>2</sup>Department of Forestry, Michigan State University, 480 Wilson Road, East Lansing, MI 48824, USA

<sup>3</sup>Departament of Forestry, Federal University of Parana\*, Pref. Lothário Meissner Avenue, 900, 80210-170 Curitiba, PR, Brazil

<sup>4</sup>Department of Science and Agroforestry Technologies, Federal University of the South of Bahia, Highway 415, km 22, 45653-919 Ilhéus, BA, Brazil

<sup>5</sup>Embrapa Forests, Road of Ribeira, km 111, 83411-000 Colombo, PR, Brazil

<sup>6</sup>Department of Forestry, Mato Grosso State University, Perimetral Deputado Rogério Silva Avenue, 78580-000 Alta Floresta, MT, Brazil

<sup>7</sup>Departament of Cartography, State University of São Paulo, Roberto Simonsen Street, n. 305, Presidente Prudente SP 19060-900, Brazil

\*Corresponding author E-mail: hassancamil@gmail.com

Received 6 February 2019

The aim of this study was to explore methods to: (1) enhance coarse-scale estimates of wood volume from National Forest Inventories (NFIs) data and (2) map them at finer scales. The ‘standard’ coarse-scale estimation extrapolates wood volume from clusters to the grid cell they represent, using the cluster’s represented forested area (RFA) to predict the cell’s forested area. Data from a subset of Brazil’s NFI clusters were combined with Landsat-8 imagery to explore a new coarse-scale method, where forested area derived from image classification (FADIC) is used instead of RFA. The RFA- and FADIC-derived estimates of total volume were, respectively, 197.4 million m<sup>3</sup> and 116.3 million m<sup>3</sup>. For fine-scale methods, volume was estimated and mapped at pixel level using: (i) surface reflectance-based models (SRMs), and (ii) regression-kriging (RK) and a RK model (RKM) whose inputs were latitude and longitude of pixels. The SRM-based method captured the mean and the general spatial trend of the volume well. The RK-based method also estimated the mean well, but it failed to predict higher and lower volumes. The SRM- and RK-based estimates of total volume were 211.7 million m<sup>3</sup> and 203.3 million m<sup>3</sup>, an overestimate of 7 per cent and 3 per cent, respectively, of the ‘standard’ NFI estimate (197.4 million m<sup>3</sup>), though both estimates were within the 95 per cent confidence interval, meaning that both fine-scale methods yield total volume statistically similar to the ‘standard’ coarse-scale method.

### Introduction

National forest inventories (NFI) provide critical information describing the amount and characteristics of forests worldwide and provide important information for decision-making about sustainable use of forest resources and the role of forests at national and global scales (McRoberts & Tomppo, 2007; McRoberts *et al.*, 2014). NFIs can be ground-based, accomplished via remote sensing or some combination of ground data and either remote sensing (Tomppo *et al.*, 2008; Gobakken *et al.*, 2012; Vibrans *et al.*, 2013) or other geographic variables (Scolforo *et al.*, 2016). Ground-based inventories were once the standard, but since the advent of remote sensing and with improvements in remote-sensing technology and spatial modelling techniques they are increasingly being applied at national,

regional and local levels (e.g. Brooks *et al.*, 2016; Maack *et al.*, 2016; Dube and Mutanga, 2015; Kim *et al.*, 2013; Lu *et al.*, 2012; Gleason & Im, 2011; Fazakas *et al.*, 1999; Cohen & Goward, 2004; Finley *et al.*, 2011). Satellite data-based models have been widely used in forestry and ecological applications, since the onset of free access to Landsat imagery (Cohen & Goward, 2004).

Recently, Brazil developed a new ground-based NFI, following a broad-scale sampling approach suited to meet national demands (Freitas *et al.*, 2010). The role of the Brazilian NFI is of special importance for supplying a permanent-plot system, with measurements of tree- and stand-level variables every five years. In its primary stages, Brazil can produce information about its forest resources at a strategic level with the NFI data; national- and regional-level maps and estimates of wood

volume are fundamental products and quantifying aboveground forest biomass (AGB) and carbon stocks plays an important role supporting greenhouse-gas emissions reporting (Kim *et al.*, 2013; Wilson *et al.*, 2013; David *et al.*, 2017). However, the current scale of the NFI data is coarse relative to what is typically needed to support forest management and planning at a regional level (Wilson *et al.*, 2013). So, methods are needed to disaggregate forest estimates from the NFI, from coarse to finer scales.

Disaggregation of Brazilian NFI data might be achieved through remote sensing-based techniques which can accurately map forest cover over broad areas (Vibrans *et al.* 2013). Some investigators have found strong relations between forest biomass and carbon with visible bands, as well as wood volume, with middle infra-red bands (Lu *et al.*, 2004), which suggests that ground inventory data from the NFI might be able to parameterize models which can extrapolate beyond the sample plot locations using information contained in the remote sensing. Kim *et al.* (2013) highlighted that suitable satellite imagery data, used in the regression analysis, must be carefully selected, given the variations in forest stand conditions and the complex relationships between spectral reflectance values. Such conditions require cautions on handling the predictor variables, examination of normality of residuals, as well as co-linearity among input variables (Hayashi *et al.*, 2015).

Kim *et al.* (2013) reviewed analytical techniques of varying complexity, combined with remote sensing, in forestry applications. Among the less-complex ones, linear regression models perhaps are among the most used (e.g. Fassnacht *et al.*, 2014), because they provide accurate results and can be rapidly processed (Lu *et al.*, 2004). Techniques such as artificial neural networks (ANN) in spatialization and mapping, often provide a little more accuracy, but depend on complex programming practices. In addition to ANN, other geostatistical techniques have been increasingly used, such as ordinary kriging, cokriging and regression-kriging (RK); this last being a hybrid method combining linear modelling with kriging (Meng *et al.*, 2009) that has been considered the most accurate alternative (Kim *et al.*, 2013).

In this study, we examined two modelling approaches to extrapolate Brazilian NFI data to map forest volume to finer (30-m pixel scale) spatial resolution. One approach extrapolated via forest cover maps derived from Landsat imagery and the other used the geographic location of forested pixels. We also examined the differences in estimated total forest volume at coarse scales (at the scale of the Brazilian NFI), when using satellite-based versus ground-inventory-based estimates of forest area. The main hypotheses of this study were: (i) that the two fine-scale methods would produce similar estimates of the total volume stocks, because their spatial resolution is the same; and (ii) fine- and coarse-scale methods would provide statistically different results of the total stock, because their spatial resolution is different.

## Materials and Methods

### Study area

The study area includes three political regions of the State of Parana, Brazil, covering ~30 per cent of the state (Figure 1). Altitudes in these regions range from 320 to 1300 m. This region fits into the Atlantic

Forest biome; the major part of the study area is covered by three forest types: Rainforest, Savanna and Seasonal Forest. According to Köppen classification, Cfa and Cfb are the predominant climate in the region, i.e. a sub-tropical climate without dry seasons, with mean temperatures higher than 22°C (Cfa) or lower than 22°C (Cfb).

### Data

Two types of data were used in this study: (i) Data from 152 NFI plots carried out in the State of Parana, Brazil, in 2013 (Figure 1), and (ii) remote sensing data for the same area.

### NFI data

The Brazilian NFI (for more complete details see, Freitas *et al.*, 2010) divides the nation into a 20 × 20 km grid of cells that are 400 km<sup>2</sup> in area. Within each cell, a sample cluster is established, shaped like a Maltese cross, with four 1000-m<sup>2</sup> subunits at the north, south, east and west (Figure 2), so that each cluster represents a small fraction of the 400 km<sup>2</sup> cell it is embedded in; we refer to this as the cluster's represented area (RA). Each cluster sub-unit is split into ten 100-m<sup>2</sup> plots, totalling 40 cluster plots. The forested area of a cluster is determined based on the number of plots that are classified as being forested, resulting in three types of clusters: (i) entirely forested clusters, when all 40 plots are categorized as forest; (ii) partially forested, when there are from 1 to 39 plots categorized as forest and (iii) non-forested, when none of the plots in the cluster are classed as forest.

Various tree variables are collected on the plots in the clusters, when visited during the inventory (Figure 2, step A); the key ones being tree stem diameter at breast height (Dbh) as well as the total height (*h*) of 12 representative trees per cluster, measured via hypsometer. Tree measurements at the plot level are used to generate plot level estimates, such as stem density, basal area and volume per forested hectare, with area extrapolated to the clusters and then to the cells.

Forested areas are divided into planted versus natural forests. For simplicity, we omitted planted forests from our analyses. Following the NFI standards, natural forests can be categorized into: (1) late-successional forest; (2) mid-successional forest with palm trees; (3) mid-successional forest without palm trees; (4) early-successional forest (ESF) with palm trees; (5) ESF without palm trees; (6) mid-successional palm forest and (7) early-successional palm forest (David, 2018). In our study area, there was no occurrence of classes 6 and 7, which are palm forest-related classes. We therefore considered only two natural forest classes that lined up with our remote-sensing approaches (see below): mid-to-late successional forests (MLSF), combined classes 1–3, and ESF, combining classes 4–5. We focused on natural forest management for timber purposes, so our target variable was stem volume of woody trees with Dbh ≥ 10 cm, i.e. we ignored palms and tree ferns (stocking only ~1.1 per cent over the total volume), as well individuals having Dbh smaller than 10 cm.

To obtain individual tree volume, we estimated via equation the total height (*h*) of the trees not measured via hypsometer. To obtain a better accuracy, we split the dataset into equal-interval *h*/Dbh strata, and then fitted stratum-specific height-diameter models, whose equations are shown in Supplementary Data 1. Next, we estimated the form factor of stems by means of species-group-specific equations; one for broad-leaved [1] and another for pine species [2]. Such equations were fitted to data (Figure 2, step B) from forests along the State of Parana.

$$f = \frac{(1.2124 \text{ Dbh}^{0.9975} h^{-0.0606})^2}{2\text{Dbh}^2} \quad (1)$$

$$f = \frac{(1.2063 \text{ Dbh}^{0.9855} h^{-0.0531})^2}{2\text{Dbh}^2} \quad (2)$$

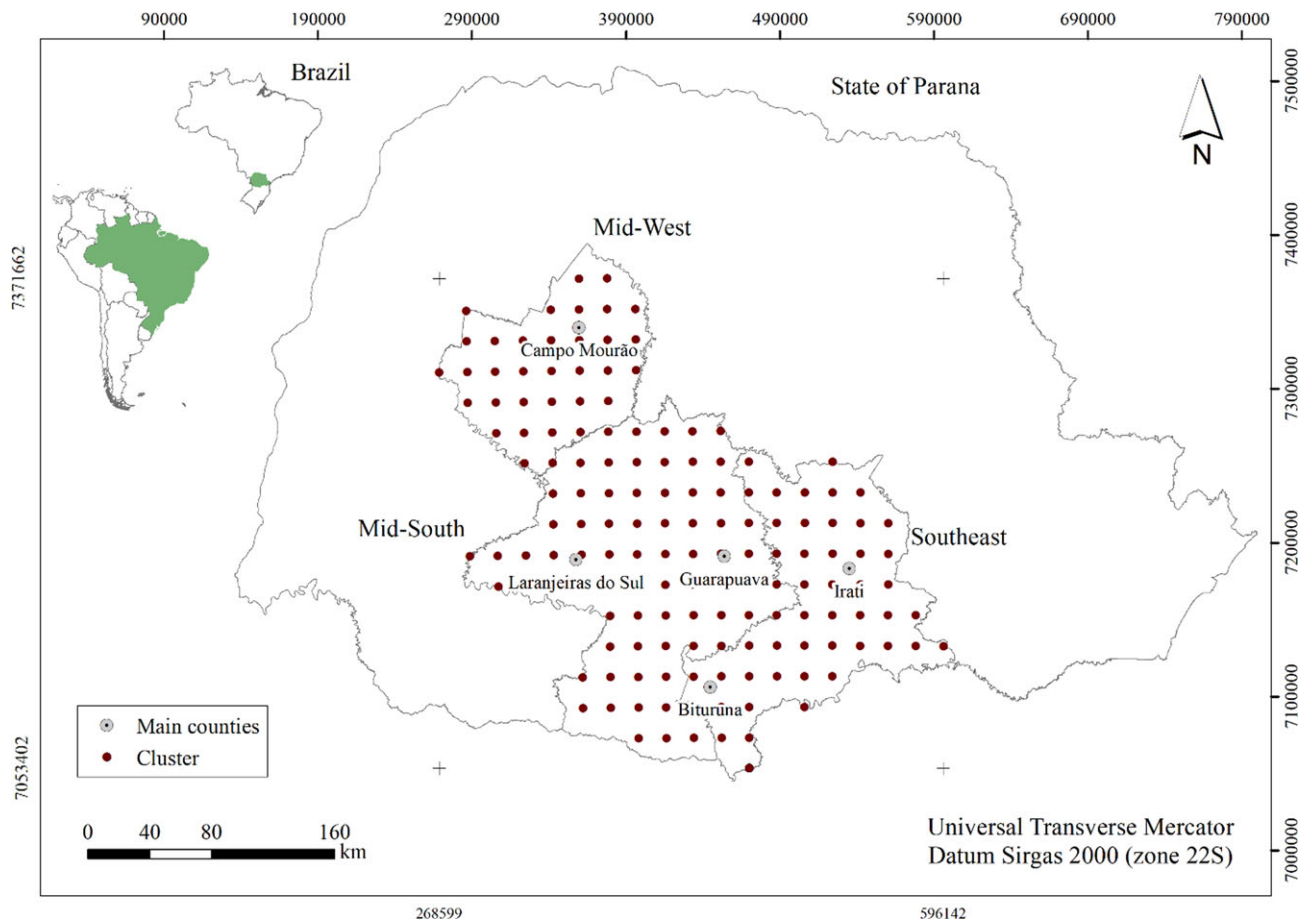


**Figure 1** Study area and location of clusters allocated following standards of the NFI sampling over the study area.

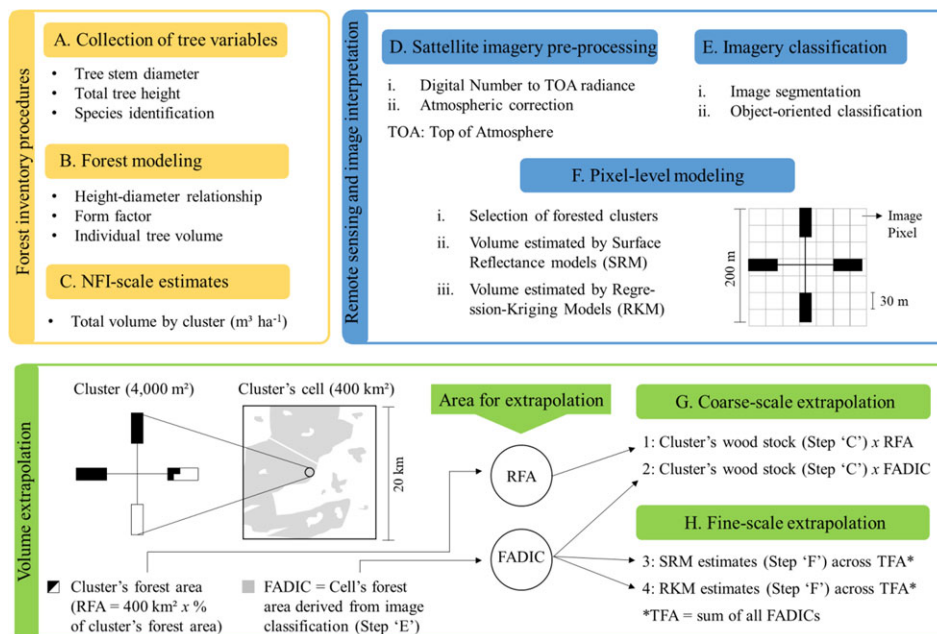


**Figure 2** Analytical procedure for estimating wood volume in natural forests at coarse and fine scales.

Stem volume was then estimated by means of the model [3]:

$$v = s_{1.3} h f \quad (3)$$

where  $v$ : stem volume (over-bark), in  $\text{m}^3$ .  $s_{1.3}$ : sectional area (over-bark) at breast height, in  $\text{m}^2$ .  $f$ : form factor. Dbh: diameter at breast height (over-bark), in cm.  $h$ : tree total height, in m.

The sum of all stem volumes (estimated through model [3]) of trees belonging to a cluster corresponds to the cluster's wood stock, given in  $\text{m}^3 \text{ha}^{-1}$  (Figure 2, step C), being our variable of interest.

Table 1 gives main statistics of total height, form factor and stem volume estimated via equations, as well Dbh and density of trees.

### Remote-sensing data

Remote-sensing data were acquired to combine with the NFI data (see Analytical procedures below). To cover the study area, seven Landsat-8 Operational Land Imager (OLI) images were obtained: (path/row) 221/077, 221/078, 222/077, 222/078, 223/076, 223/077 and 223/078, all downloaded from the US Geological Survey (USGS). The period from December 2013 to February 2014 was chosen to acquire the satellite imagery, because it provides cloud cover lower than 0.25 per cent for all images and aligns with the period when the NFI data were collected. Imagery pre-processing was performed with Envi 5.3, being: (i) conversion of digital number to radiance scale, and (ii) conversion of radiance to surface reflectance (Figure 2, step D), this last executed with Fast Line-of-sight Atmospheric Analysis of Hypercubes (FLAASH) algorithm, implemented in Envi 5.3. FLAASH is based on the MODTRAN-4 radiative transfer (Berk *et al.*, 1999) for performing atmospheric correction necessary to remove most of the haze and other atmospheric perturbations (Nazeer *et al.*, 2014). After this, the (iii) images were re-projected to Sirgas 2000 and (iv) clipped for removing overlapped borders from neighbour scenes.

### Analytical procedures

The analytical procedures are summarized in Figure 2 and described in detail below. Data acquisition and pre-processing steps were described in the previous sections (Figure 2, steps A–D).

### Image segmentation and classification

The images were segmented and classified (Figure 2, step E) by using the software eCognition Developer 8.7 (Trimble, 2011). This software

executes object-oriented classification, where ‘objects’ are a definite spatially-connected region of the satellite image. The object-oriented classification approach we used prevented expression of a ‘salt-and-pepper’ effect (Blaschke, 2010) that is often associated with pixel-based classifications. eCognition Developer 8.7 allows users to segment imagery by means of seven different algorithms; the ‘multiresolution segmentation’ algorithm was chosen for this research. This algorithm applies an optimization procedure for locally minimizing the average heterogeneity of objects. This procedure requires that image layers and weights ( $w$ ) for each layer be chosen as segmentation criteria, besides parameters referring to size (scale), shape, and compactness of the image objects. For this research, all the seven images were segmented using the same standardized parameters and image  $w$ , as well as the same image layers: SWIR1 (Layer 1), NIR (L2) and Red (L3). After performing an exploratory analysis changing  $w$ , parameters, and layers, the largest weight ( $w = 1.6$ ) was assigned to SWIR1 (i.e. Layer 1), followed by NIR (Layer 2,  $w = 1.0$ ) and Red (Layer 3,  $w = 0.6$ ) (Figure 8). The values for the parameters shape and compactness were 0.1 and 0.5, respectively.

After the segmentation process, we classified the imagery considering land-use classes. As our variable of interest was wood volume stocks in natural forests, the classification was focused on identifying areas occupied by natural forests throughout the study area, though other land-uses classes also had to be considered, as described later. Franklin (2001) addressed the importance of accomplishing forest classification under a hierarchical structure and the software we used allows that classes be hierarchically structured, such that a ‘child class’ inherits descriptions from its ‘parent’ class. The parent classes were (I) forest and (II) non-forest. Class II was the inverted expression for class I, such that objects not classified as forest turned into non-forest automatically (an option provided by eCognition Developer 8.7). The child classes associated with (I) were (i) early-successional natural forests, (ii) mid- to late-successional natural forests and (iii) planted forests. The two classes of natural forests were created based on the Resolution n. 2 from CONAMA (Brasil, 1994); a Brazilian standardization that defines and characterizes early- and mid-to-late forest types. Although the volume of planted forests was ignored, the land-use class ‘planted forests’ was included in the image classification for completeness and to improve classification accuracy, to help reduce misclassification between natural and planted forests. It was also necessary to create another child class for patches of lowland natural forests, which are generally areas wetter than the higher ones and consequently have different spectral response from the infra-red bands (NIR, SWIR1, SWIR2). An amount of 10 000–20 000 samples (by scene, by class) of image objects (result from image segmentation) were collected to represent parent and child classes.

**Table 1** Descriptive statistics of tree variables by group of species, in NFI plot data of the State of Parana.

Tree variable	Minimum	Medium	Maximum	CV (%)
Broad-leaved species – $n$ : 10 822 individuals				
Diameter at breast height (cm)	10.0	18.4	118.3	52.0%
Total height (m)	1.4	10.4	28.0	34.9%
Form factor <sup>a</sup>	0.481	0.551	0.696	4.8%
No. of trees $\text{ha}^{-1}$ (Dbh $\geq 10$ cm) <sup>b</sup>	3	237	1208	91.4%
Stem volume ( $\text{m}^3 \text{tree}^{-1}$ ) <sup>a</sup>	0.009	0.228	9.512	189.0%
Pine species – $n$ : 526 individuals				
Diameter at breast height (cm)	10.0	27.1	74.8	53.5%
Total height (m)	4.0	13.4	26.0	32.5%
Form factor <sup>a</sup>	0.458	0.508	0.587	4.7%
No. of trees $\text{ha}^{-1}$ (Dbh $\geq 10$ cm) <sup>b</sup>	3	53	1315	350.0%
Stem volume ( $\text{m}^3 \text{tree}^{-1}$ ) <sup>a</sup>	0.020	0.580	4.831	128.1%

<sup>a</sup>Values obtained through equations previously described. <sup>b</sup>Average per cluster. CV, coefficient of variation;  $n$ , number of observations.



Five variables related to the image layers were chosen for the image classification: (i) brightness index, (ii) mean SWIR1, (iii) mean NIR, (iv) NDVI and (v) maximum difference of the image objects. The brightness index plays the role of a proxy variable and is defined as the mean reflectance of SWIR1, NIR and Red of an image object, as proposed by the software. This same brightness index was used in the reflectance models described later. For the sake of simplicity, brightness index is just called 'brightness'. NDVI is the Normalized Difference Vegetation Index usually applied in vegetation studies with remote-sensing data (Powell *et al.*, 2010).

A post-classification visual analysis was accomplished to manually edit misclassified objects (including shadow misclassification) to improve the classifications. The accuracy of the classifications was assessed by means of confusion matrices for each of the images and the Kappa index of agreement, as explained by Congalton & Green (2008). To better help understand the distribution of forests, as well of large forested and deforested regions, we also presented a ground slope map originated from SRTM (30-m spatial resolution), as proposed in Weber *et al.* (2004), because we observed elevation patterns in the forest distribution.

### Coarse-scale estimation of wood volume

The first coarse estimation method was to directly extrapolate the total wood volume ( $\text{m}^3 \text{ha}^{-1}$ ) over the study area (Figure 2, step G1); this is essentially the 'standard' method currently provided by the Brazilian NFI data. The natural forest volume per ha observed in entirely- or partially-forested clusters during the NFI was multiplied by an extrapolation factor relating the percent forest in the sample cluster to the cell it represents, which we refer to as the represented forested area (RFA). For entirely forested clusters, the estimated RFA is  $400 \text{ km}^2$  (assuming that the entire cell is 100 per cent forested). For partially-forested clusters, the estimated RFA is proportional to the cluster's forested area; for example, if 50 per cent of a cluster is in forest, RFA is  $200 \text{ km}^2$  (assuming that half of the cell is considered forested). For non-forested clusters, the estimated RFA is  $0 \text{ km}^2$  and consequently the extrapolation is set to 0. So, the total RFA for the study area is the sum of the RFA estimated for each cell. The total volume over the study area is the sum of the products of the wood volume of each cluster and its RFA. Since the mean and standard error of volume per cluster was known, it was possible to obtain confidence intervals (CI) of the total volume; we applied the method of the first differences for systematic sampling, as described in Chacko (1965).

To understand how the remote-sensing data might change the coarse-scale volume estimate, we computed a second estimate, using another method (Figure 2, step G2), where the same volume estimates for the clusters are used, but they are extrapolated to the forested area of entire cells derived from image classification (FADIC); therefore, the total forest area is computed at the cell, rather than cluster level, and disregards the cluster's RFA. Each cluster had its own FADIC, so that the sum of all FADICs is the total forested area (TFA) resulted from the image classifications. So, the remote-sensing extrapolated estimate of total volume over the study area is the sum of the products of the wood volume of each cluster and the cell's FADIC.

In summary, the coarse-scale methods differ each from other by the method of estimating the extrapolation area: RFA and FADIC. In an ideal situation, the proportion of forest of the clusters would be equal to the proportion of forest over the  $400\text{-km}^2$  cell, i.e. RFA would be equal to FADIC. Under such a situation, both coarse-scale methods would estimate the same total volume, confirming the consistency between both coarse methods. However, since the NFI clusters are only  $0.004 \text{ km}^2$ , we expected that the cluster would be unlikely to match the actual proportion of forest in the cell (Figure 2). The coarse-scale estimation was computed for both methods for both totally and partially forested clusters

and we compared the estimates from both methods to examine how large the difference, if any, there was.

### Fine-spatial-scale estimation of wood volume

We tested two fine-scale methods (Figure 2, step H) that produced wood volume estimates for each  $30\text{-m}$  pixel in the study area. The first method (Figure 2, step H3) consisted of estimating wood volume as a function of reflectance pixel data, with application of a model we refer to as 'surface reflectance-based model' (SRM). The second method (Figure 2, step H4) had application of RK and of the RK model (RKM) as a function of pixel locations (lat./long.). The latter was chosen because latitude and longitude are variables that are much easier to obtain than reflectance values from remote sensors, so it represents a more easily-implemented approach to extrapolating over space. Both the SRMs as the RKM were employed with two randomly selected sub-datasets: (i) fitting, with  $\sim 90$  per cent of the data participating in the model calibration and (ii) validation, with  $\sim 10$  per cent of the data.

### Surface reflectance-based model

The SRM (Figure 2, step F) determined wood volume ( $\text{m}^3 \text{ha}^{-1}$ ) of clusters from surface reflectance pixel values from Landsat-8 OLI bands. To fit the SRM, data consistency was necessary to eliminate outlier pixels that do not represent the variable of interest, as discussed by Fazakas *et al.* (1999). This occurs because the localization of the clusters on the ground is not exactly the same location on the digital maps, due to Global Positioning System (GPS) errors, and to the fact that the surface reflectance of pixels suffers from the influence of neighbouring pixels (Maack *et al.*, 2016). In this study, such influence was most likely to occur where pixel reflectance values of clusters along the border of forests were affected by non-forested pixels (Hall *et al.*, 2006). The rule employed removed lower and upper outlier pixels from the dataset if the pixel value was lower or higher, respectively, than 1.5 times the inter-quartile range of reflectance values.

The input (image value) and output (cluster volume) variables were extracted at pixel level through Geographic Information System (GIS) analysis. The chosen image bands were: Red, NIR, SWIR1, SWIR2, Brightness and NDVI. Stepwise regression was used to select the most important input variables, leaving variables that were statistically significant ( $\alpha \leq 5$  per cent) and removing those non-significant ones. The Shapiro-Wilk statistic for testing the normality indicated that the input variables were normally distributed at a 5-per cent probability level.

Satellite sensor data are commonly correlated (Hayashi *et al.*, 2015). To fix this problem, the raw input variables (i.e. surface reflectance) were transformed into principal components (PCs), which is one of the most commonly-used transformations for satellite data (Meng *et al.*, 2009). In the principal components analysis (PCA), PCs with significant eigenvalues capture the largest amount of variance of raw data (Johnson & Wichern, 2007), therefore, only these PCs were used in the regression analysis. The SRM was fitted through the method of ordinary least squares and can be expressed by [4]:

$$\hat{V}_i = \alpha_0 + \alpha_1 PC_{i1} + \alpha_2 PC_{i2} + \dots + \alpha_j PC_{ij} + \varepsilon_i \quad (4)$$

in which PC is given by [5]:

$$PC_{ij} = \beta_1 X_{i1} + \beta_2 X_{i2} + \dots + \beta_p X_{ip} \quad (5)$$

Where,  $\hat{V}$ : wood volume,  $\text{m}^3 \text{ha}^{-1}$ . PC: principal component. X: raw input variable. j: number of PCs with  $\lambda \geq 1$ . p: number of variables selected by stepwise.  $\alpha_j$ : coefficients of the volume model.  $\beta_j$ : coefficients of the PC.  $\varepsilon_i$ : random error.

Each one of the seven Landsat scenes had the model [4] fitted to them by using the specific dataset of clusters related to each scene.

Separation by scene was necessary due to the variation of reflectance values among them, caused by solar illumination, haze and atmospheric conditions, among others. The equations from Landsat scenes 223/076 and 223/078 were replaced by similar equations from bordering scenes, due to the lack of or low number of forested pixels, yielding thus five SRM equations. With the raster files containing surface reflectance data, these equations were used to estimate wood volume at pixel level by using the raster calculator available in Envi 4.7, creating a raster file of estimated wood volume.

The last step was to clip raster files by using vector files from the image classifications. As these vector files delimit forest and non-forest patches, clipping removes all pixels out of forest, generating a map of natural forests across the study area.

### Regression-kriging and RK model

RK is a geostatistical, hybrid method that combines kriging with a RK model (RKM) (Odeh et al., 1995). The role of the RKM (Figure 2, step F) is to introduce regression residuals into the spatial analysis (Meng et al., 2009), i.e. into the spatialized variable (in this case wood volume). The main idea was to take advantage of the capability of the RK method in fixing estimated values with addition of spatialized residuals. To contrast with the SRM, volume was modelled as a function of latitude and longitude (as shown in [6]), instead of using reflectance data, to determine if location, as a proxy for local climate, could provide a simpler way to extrapolate NFI plot data. Mello et al. (2015), Scolforo et al. (2015) and Angulo-Martínez et al. (2009) are examples of other studies that employ RKMs in this context. The specific model employed was:

$$\hat{V}_i = \alpha_0 + \alpha_1 X_i + \alpha_2 Y_i + \varepsilon_i \quad (6)$$

where  $\hat{V}$ : wood volume of a pixel, in  $\text{m}^3 \text{ha}^{-1}$ .  $X$ : latitude of a pixel.  $Y$ : longitude of a pixel.  $\alpha_i$ : regression coefficients.  $\varepsilon_i$ : random error.

Before executing the RK, we fitted the RKM [6] and obtained residuals ( $r_i$ ) of wood volume by the formula  $r_i = y_i - \hat{y}_i$ , where  $y_i$  is the observed wood volume and  $\hat{y}_i$  is the wood volume estimated by the RKM. To fit the RKM, three assumptions were considered:  $E(r_i) = 0$ ,  $\text{Cov}(r_i, y_i) = 0$  and  $\text{Cov}(r_i, x_i) = 0$  (Odeh et al., 1995). After that, an Exponential Model [7] was fitted to the semivariogram of the residuals ( $r_i$ ). The function *variofit* from the GeoR package was used for fitting the semivariogram (Ribeiro Junior & Diggle, 2001).

$$\gamma(h) = \tau^2 + \sigma^2 \left[ 1 - e^{-\left(\frac{h}{\varphi}\right)} \right] + \varepsilon_i \quad \text{for } h < \varphi \quad (7)$$

$$\gamma(h) = \tau^2 + \sigma^2 + \varepsilon_i \quad \text{for } h \geq \varphi$$

where  $\gamma(h)$ : semivariance.  $\tau^2$ : nugget effect.  $\sigma^2$ : random variance.  $h$ : distance between clusters, in km.  $\varphi$ : range;  $e$ : exponential.  $\tau^2 + \sigma^2$ : sill of the semivariogram.  $\varepsilon_i$ : random error.

The spatial dependence of the regression residuals was quantified by means of the ratio ( $r(h)$ ) between nugget effect and sill. The value of  $r(h)$  was then classified into three classes of spatial dependence, as proposed by Cambardella et al. (1994).

$$r(h) = \frac{\tau^2}{\tau^2 + \sigma^2} 100 \quad (8)$$

An exponential model was applied to spatialize the regression residuals at pixel level, in which the final product was a 30-m spatial resolution raster. Subsequently, the wood volume was also spatialized at pixel level, but now using the RKM. To that end, a vector format file containing points with latitude and longitude from each image pixel was required for the wood volume estimation. This operation also produces a 30-m spatial resolution raster. These two raster files were added each other aiming to sum, at pixel level, regression residuals and estimated

wood volumes. Procedures for clipping rasters to obtain map of wood volume is similar to the SRM case. These methods have a same extrapolation area, which is the FADIC.

### Uncertainty analysis

We quantified uncertainty in the wood volume ( $\hat{V}_i$ , in  $\text{m}^3 \text{ha}^{-1}$ ) estimation by means of the Monte Carlo method (MCM), following, e.g. McRoberts et al. (2015) and Finley et al. (2011). As we modelled  $\hat{V}_i$  at pixel level from two different models (SRMs and RKM), the uncertainty analysis was applied to each of these cases. The MCM is an approach that relies on the distribution of data, in our case, normal distribution. Our procedure is summarized in four steps: (i) obtaining standard deviation of  $\hat{V}_i$  (i.e.  $\sigma_{\hat{V}}$ ), and a size- $n$  vector of predicted volumes (i.e.  $\hat{V}_i$ ); (ii) generating vector of random values (i.e.  $\hat{X}_i$ ) based on  $\sigma_{\hat{V}}$  and  $\hat{V}_i$ , with  $\hat{X}_i$  representing wood volume simulations forced to follow the normal distribution; (iii) replicating steps (i) and (ii) 5000 times; and (iv) binding the 5000  $\hat{X}_i$  into an only one vector, for calculating standard deviation of  $\hat{X}_i$  (i.e.  $\sigma_{\hat{X}}$ ).

These four steps were performed five times for the SRM, because it was fit to five image scenes, and one time for the RKM, because it was fit to a single data frame. So,  $\hat{V}_i$  obtained in step (ii) is generated both from the SRM and the RKM, with each having a different number of observations ( $n$ ), which is a parameter we used to determine the size of  $\hat{V}_i$  (step i), so that  $\sigma_{\hat{X}}$  be proportional to the size of datasets.

By observing the total amount of pixels in the forest map, we computed the mean wood volume ( $\bar{v}_p$ ) at pixel level, in  $\text{m}^3 \text{ha}^{-1}$ . The aim of the analysis was to obtain an CI with the new standard deviation fixed by the uncertainty,  $\sigma_{\hat{X}}$ . The CI for the total wood volume is  $TFA (\bar{v}_p \pm t\sigma_{\hat{X}}/\sqrt{n})$ .

### Assessment of goodness-of-fit

Goodness-of-fit statistics were applied to the pixel-level models [4] and [6] aiming to examine their accuracy. The SRMs were fitted, by scene, to evaluate the accuracy of the global volume estimation, so statistics were proportionally weighed in relation to the portion that each Landsat scene covered the study area. The accuracy statistics were: adjusted coefficient of determination [9], root mean square error (%) [10], mean error (ME) [11] and mean absolute error [12]:

$$R_{adj}^2 = 1 - \left[ \frac{\sum_{i=1}^n (y_i - \hat{y}_i)^2}{\sum_{i=1}^n (y_i - \bar{y})^2} \left( \frac{n-1}{n-p} \right) \right] \quad (9)$$

$$RMSE(\%) = \frac{1}{n-p} \left[ \sum_{i=1}^n (y_i - \hat{y}_i)^2 \right]^{\frac{1}{2}} \frac{100}{\bar{y}} \quad (10)$$

$$ME = \frac{1}{n} \sum_{i=1}^n (y_i - \hat{y}_i) \quad (11)$$

$$MAE = \frac{1}{n} \sum_{i=1}^n |y_i - \hat{y}_i| \quad (12)$$

where  $y$  is observed volume,  $\hat{y}$  is predicted volume,  $\bar{y}$  is mean observed volume,  $n$  is number of observations and  $p$  is number of parameters.

## Results

### Image classification

The vegetation map resulting from the image classification is presented in Figure 3. The total area classified as 'ESF' and

'MLSF' were 432 528 ha and 1 330 041 ha, respectively. These two classes combined totalled 1 762 570 ha of TFA, i.e. sum of all FADICs (Table 2).

The map of ground slope in Figure 3 indicates that most forests are located on steeper terrain, and vice versa for non-forest. The image classifications yielded Kappa values ranging from 0.81 to 0.90 (see Supplementary Data 2), which corresponds to a relatively strong agreement between the imagery and the ground truth (Landis & Koch, 1977). In general, disagreements were mostly classes of non-forest (e.g. tillage, pasture) being erroneously classified as ESF, but also planted forests were misclassified as both ESF and MLSF, and vice versa.

### Coarse-scale estimation of forest area and wood volume

Table 2 shows forest area estimates and volumes for the study area extrapolated via RFA computed from the NFI sample clusters of via the FADIC. Recall that the total area represented by each cluster is 400 km<sup>2</sup> and 152 clusters were examined, so the total area represented (RA) is 6 080 000 ha (152 × 40 000 ha). Summing the forested areas of the entirely and partially forested clusters from the NFI data, the overall RFA was 1 987 000 ha, which corresponds to an overall forest coverage of 32.7 per cent (=RFA/RA), coming from 100 per cent coverage in the

entirely-forested clusters and an estimated forested cover of a little under 50 per cent for the partially-forested clusters (Table 2). Multiplying the mean volume per ha in each type of sample cluster (Table 2) by the RFA for each cluster led to an estimated total volume of 197 396 519 m<sup>3</sup> (± about 5000 m<sup>3</sup>, 95 per cent CI) over the study area.

The FADIC from Landsat, by contrast, indicated that only about 35 per cent of the area represented by entirely-forested clusters from the NFI was actually forested, and only about a third of the area represented by the partially-forested clusters; this led to much less volume predicted in those areas (Table 2). Additionally, the FADIC was almost 500 kha in the cells containing non-forested NFI clusters. This resulted in a total FADIC (TFA, Table 2) about 11 per cent less than the total forest area predicted by the NFI data (total RFA, Table 2), because the imagery suggested that there was significant forested area in the cells containing non-forested clusters, which mostly compensated for the lower levels of forested area suggested to be in the cells containing forested sample clusters. On the other hand, the total estimate of forest volume from forested NFI clusters extrapolated via FADIC was about 41 per cent less, due to the mismatch between the forested volume represented by the different types of sample clusters and the RFA versus FADIC (Table 2).

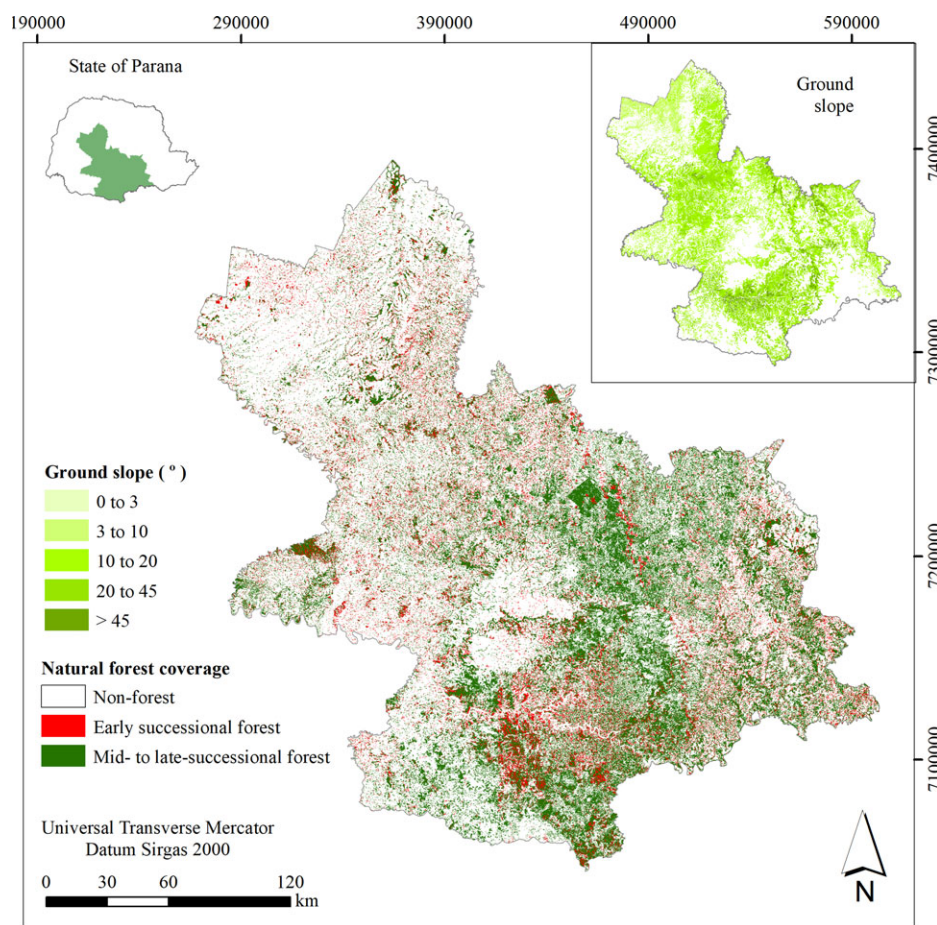


**Figure 3** Spatial distribution of early-successional and mid- to late-successional forests and ground slope in a study area within the State of Parana, Brazil.



### SRM and RKM model performance

Table 3 gives goodness-of-fit statistics from the SRMs and the RKM. As proposed, each Landsat scene had its specific SRM. The overall RMSE was of 32.5 per cent for the SRM-based estimation, ranging from ~29 to 51 per cent for the individual scenes. The RKM-based estimation had a higher error at 49.0 per cent RMSE.

The results for the fitting and validation datasets were very similar, which indicates that the validation dataset was a good representation of the overall dataset.

The RKM was less accurate than the SRMs (Table 3). However, we reiterate that the RKM does not provide the final wood volume estimates. Instead, the final estimates are obtained by adding spatialized estimates from the RKM to their respective

**Table 2** Total forest area and volume estimates based on NFI sample clusters versus those extrapolated via forest classification from the satellite imagery.

Statistics	Unit	Type of sample cluster			
		Entirely forested (A)	Partially forested (B)	(C) Non-forested	Total (A + B + C)
Number of clusters	<i>n</i>	7	89	56	152
Proportion of clusters	%	4.60	58.60	36.80	100.00
Area represented by NFI sample clusters (RA)	ha	280 000	3 560 000	2 240 000	6 080 000
Forest area and volume estimates from NFI sample clusters					
Forested area represented by NFI sample clusters (RFA)	ha	280 000	1 707 000	0	1 987 000
Proportion of forest coverage (=RFA/RA)	%	100.00	47.95	0.00	32.68
Lower total volume ( $\alpha=5\%$ )	m <sup>3</sup>	55 603 212	109 703 290	0	165 306 502
Total volume	m <sup>3</sup>	60 639 475	136 757 044	0	197 396 519
Upper total volume ( $\alpha=5\%$ )	m <sup>3</sup>	65 675 737	163 810 798	0	229 486 535
Forest area from image classification and volume estimates from NFI sample clusters					
Forested area delimited by image classification (FADIC)	ha	97 987	1 186 667	477 916	1 762 570 <sup>a</sup>
Proportion of forest coverage (=FADIC/RA)	%	35.00	33.33	21.34	28.99
Lower total volume ( $\alpha=5\%$ )	m <sup>3</sup>	19 461 278	76 248 504	0	97 386 291
Total volume (forested clusters)	m <sup>3</sup>	21 223 984	95 052 027	0	116 291 341
Upper total volume ( $\alpha=5\%$ )	m <sup>3</sup>	22 986 690	113 855 549	0	135 196 391

<sup>a</sup>Total Forested Area (TFA) includes FADIC in cells containing non-forested clusters.

**Table 3** Goodness-of-fit statistics of the pixel-level models SRM and RKM predicting total volume.

Scene	Dataset	$R^2_{\text{adj.}}$	RMSE%	ME <sup>a</sup>	MAE <sup>a</sup>	DF	Coverage <sup>b</sup> (%)
Surface reflectance-based model (SRM)							
221/077	Fitting	0.61	30.7%	0.00	46.33	41	3.4
	Validation	0.59	31.5%	18.78	37.64	4	
221/078 and 223/076	Fitting	0.11	27.4%	0.00	20.73	299	24.3
	Validation	0.10	33.0%	−5.64	23.86	43	
222/077 and 223/078	Fitting	0.33	39.3%	0.00	36.56	283	23.0
	Validation	0.32	41.8%	12.35	41.10	36	
222/078	Fitting	0.39	28.9%	0.00	33.08	542	44.0
	Validation	0.39	29.0%	9.86	34.59	77	
223/077	Fitting	0.22	41.9%	0.00	49.53	66	5.4
	Validation	0.18	51.0%	8.73	36.08	7	
Overall	Fitting	0.43	32.5%	−1.57	33.05	1231	100
	Validation	0.46	32.3%	−6.84	33.53	167	
Regression-kriging model (RKM)							
Overall	Fitting	0.11	49.0%	0.00	41.55	60	100
	Validation	0.11	47.2%	−13.23	26.57	10	

<sup>a</sup>Value given in m<sup>3</sup> ha<sup>-1</sup>. RMSE, root mean square error; ME, mean error; MAE, mean absolute error; DF, degrees of freedom. <sup>b</sup>Coverage by scene over the study area.

spatialized regression residuals. In other words, the RMSE of the RKM (Table 3) does not portray the overall accuracy of the final estimates.

Figure 4a,c show plots of estimated and observed volumes for both SRM and RKM. Figure 4a indicates a moderate tendency in overestimating the lower volumes by the SRM, and underestimating the higher ones, but otherwise predicted and observed values are roughly linearly related. RKM, by contrast, showed a relatively constant estimated volume over the range of observed volumes. This occurred because latitude was the only significant ( $P$ -value < 5 per cent) variable in the RKM fitting and the spatial pattern of wood volume was apparently much more complex than a simple latitudinal gradient.

The accuracy of the RK depends on residuals (of the RKM) following the normal distribution pattern, once normality is a condition necessary to apply the technique (Odeh *et al.*, 1995). Figure 4b,d reveal a distribution of the regression residuals for both methods approaching normality and the Shapiro-Wilk test confirms that the residuals from both models are normally distributed at 95 per cent probability level. This indicates that many of the positive and negative residuals nullify themselves. However, both methods show an overall error in predictions, as indicated by the ME for the validation data, and with a lower error for the fitted models than the validation data, as expected (Table 3).

In addition to normality, another issue of importance for the application of the RKM is that the regression residuals have spatial dependence further than ~20 km, which is the minimum distance among clusters. The practical asymptotic range (95 per cent of the sill) of the Exponential Model [7], which is equal to three times the value of range ( $\phi$ ) (Wackernagel, 2003), was of 269.6 km, meaning that there is spatial dependence until such distance. With this result, the residuals could be properly spatialized with the NFI grid distance. Residuals were classified as moderately spatially dependent ( $r(h) = 55.32$  per cent). The equation of the semivariogram is expressed in [13].

$$\gamma(h) = 16.3804 + 13.2294 \left[ 1 - e^{-\left(\frac{h}{90,000}\right)} \right] \quad (13)$$

where  $\gamma(h)$ : semivariance;  $h$ : distance between clusters;  $e$ : exponential.

### Fine-scale estimation of wood volume

Each method (SRM and RKM) estimated wood volume at pixel level and the frequency distribution of pixels classes of volume are presented in Figure 5. The SRM produced a frequency of volumes much close to a normal distribution and covered a full

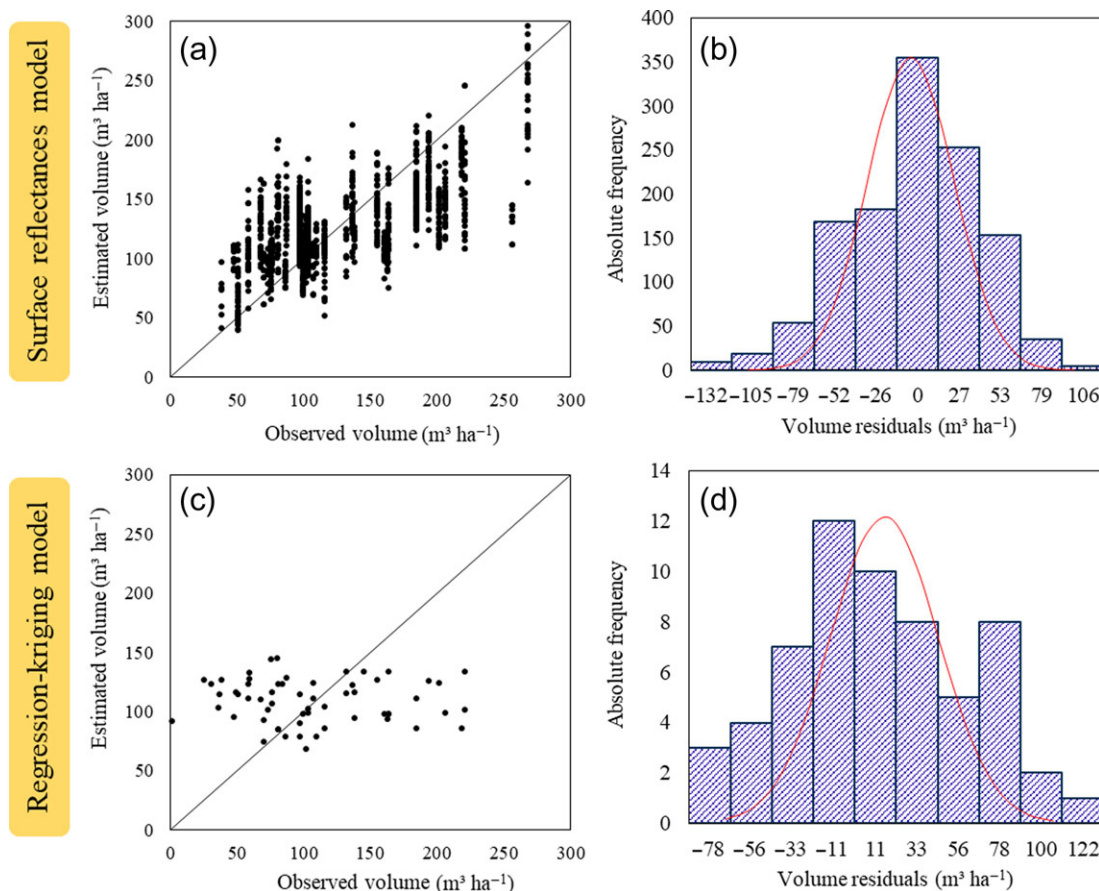


**Figure 4** Graphs showing estimated x observed volumes (a, c) and histogram of residuals of volume estimates (b, d). Red line: normal distribution curve.

range of values reflected in the ground-based observations from the NFI. In contrast, RKM predicted a much more limited range of volume with very high frequencies for some volume classes (Figure 5).

Ultimately, the goal was to produce a fine-scale map of forest volume; the resulting maps describing the spatial distribution of the wood volume ( $\text{m}^3 \text{ha}^{-1}$ ) estimated through both methods is shown in Figure 6. The maps show a spatialized representation of the data shown in Figure 5. In general, both maps agree on where the densest areas of forest volume are, but the SRM suggests a greater variety of volumes and a greater spatial differentiation across the landscape.

The last result was the total wood volume estimated for the study area under each extrapolation method, which is total volume of all the pixels, under each method, including the 95 per cent CI from the uncertainty analyses (Table 4). Both the SRM and the RKM produced higher total volume estimates for the landscape than that suggested by the NFI (compare Tables 2 and 4). We noted that the CI provided by the SRM-based method (Table 4) fits into and is more precise than the CI yielded by the 'standard' NFI method (Table 4). The CI provided by the RKM-based method, in turn, had the upper limit slightly exceeding in relation to the CI of the 'standard' method; however, it was less precise than the CI of the SRM. The relative

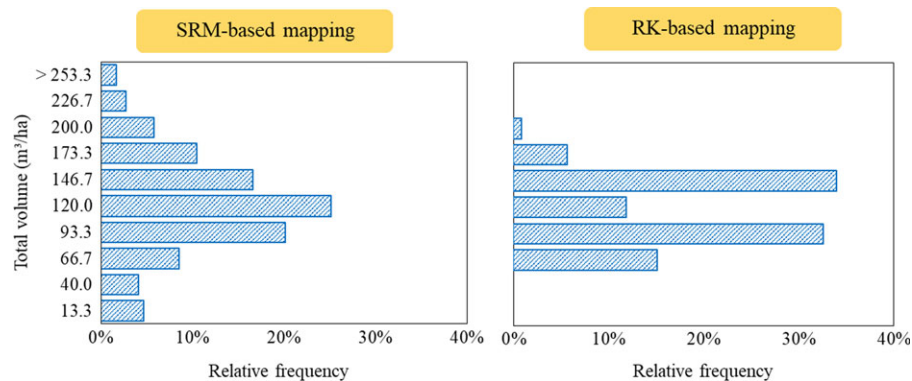


**Figure 5** Frequency of pixels versus classes of wood volume estimated by pixel-level methods of mapping.

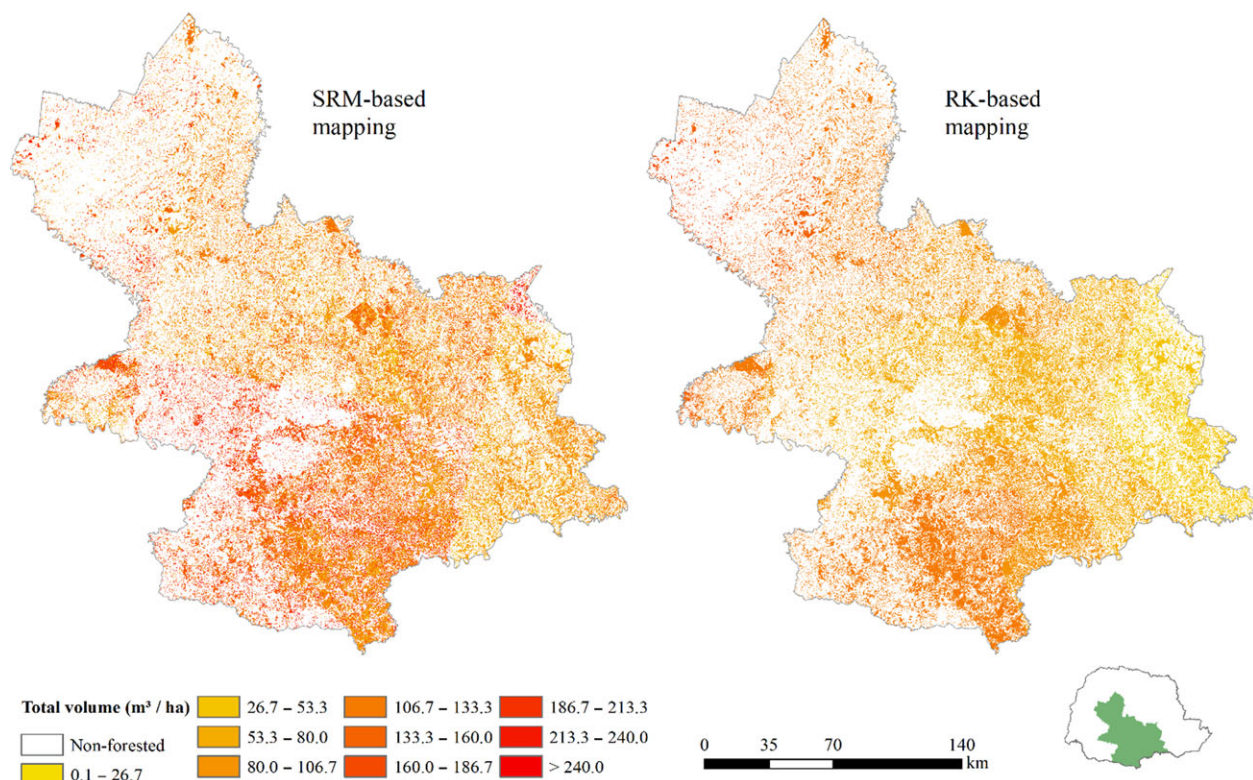


**Figure 6** Spatial distribution of the volume estimated by the methods with SRM and RK.



**Table 4** Total wood volume estimated from the SRMs and RKM, and CI obtained from the uncertainty analysis.

	Unit	SRM	RKM
Lower total volume ( $\alpha=5\%$ )	m <sup>3</sup>	201 540 889	176 633 239
Total volume	m <sup>3</sup>	211 703 516	203 326 674
Upper total volume ( $\alpha=5\%$ )	m <sup>3</sup>	221 866 144	230 020 109

volume estimation errors ( $\pm$ standard error/estimate) were: SRM =  $\pm 5$  per cent; RKM =  $\pm 13$  per cent. Table 4 gives the CIs provided by the two methods.

## Discussion

### Coarse-scale estimates of volume given different estimates of forest area

The large discrepancy in the total volume is between the 'standard' NFI estimate (197 396 519 m<sup>3</sup>) and that one based on the image classification (116 291 341 m<sup>3</sup>, Table 2), result from the large difference between RFA and FADIC. The cells containing 'entirely-forested' clusters were not entirely forested as estimated by FADIC. This result reflects the fact that our study area is a region with fragmented vegetation, with no occurrence of 400-km<sup>2</sup> cells that are actually entirely forested. In general, FADIC should be lower than RFA in cells containing entirely-forested clusters, except perhaps in well-forested regions of Brazil's Amazon, where large contiguous forested areas are found. For the cells containing partially-forested ones, we expected a better match between FADIC and RFA.

The most important difference between RFA and FADIC was in cells containing non-forested clusters, where almost 500 k ha of forest was estimated by FADIC (Table 2). A partial explanation for the discrepancy could be from non-forested areas (e.g. tillage, pasture) erroneously classified as ESF, which was the major source of error over the image classification (see Supplementary Data 2). This error in the classification was caused because some image objects belonging to agricultural areas shared the same spectral range with objects from young forest vegetation, as shown in Trishchenko *et al.* (2002) and Kachhwaha (1983). Though there may have been some misclassification error, our results suggested a considerable amount of wood volume might be present in cells containing non-forested clusters. This highlights the importance of correctly identifying non-forested and forested areas to derive accurate estimates and maps of forest attributes over large spatial domains (see Finley *et al.* 2011).

Overall, this part of our analysis revealed a mismatch between the % forest cover in a cell and the % forest cover of a sample cluster representing it. The NFI cluster represents an area one hundred thousand times the plot size. By contrast, the US NFI has a ratio of plot area to RA of 1:6000 (Bechtold and Patterson 2005). The relatively small size of the NFI sample cluster (0.001 per cent of the cell), gives a high probability that a non-forested cluster could land in a partially-forested cell, or vice versa. While this does not mean that the RFA is biased at the national level, based on the NFI design, it does suggest a

strong need to enhance estimates with remote-sensing data at smaller scales.

### Performance of the SRMs for estimating wood volume at pixel level

Many authors have modelled forest variables as a function of remote-sensing data (Fazakas *et al.*, 1999; Krankina *et al.*, 2004; Labrecque *et al.*, 2006; Kim *et al.*, 2013; Maack *et al.*, 2016; Bohlin *et al.*, 2017). The SRM method we tried in the study area, appeared to be an effective method for extrapolating wood volume to finer spatial scales than are currently possible, using remote-sensing data, combined with the NFI data. Our SRMs had relatively good performances (Table 3) comparing to some other studies reported in the literature. As examples, Berra *et al.* (2012), Mäkelä & Pekkari (2004), and Mohammadi *et al.* (2010) used Landsat imagery to estimate wood volume in homogeneous forests, obtaining RMSE ranging from 48 per cent to 100 per cent. In deciduous forest, Tomppo *et al.* (2002) found up to 180 per cent of error in volume estimates. Aiming at estimating AGB in across the Northern Minnesota, US, Deo *et al.* (2017) used remotely-sensed data from Landsat and Lidar to test various pixel-level polynomial models. The authors found RMSE ranging from ~35 to ~70 per cent. Fazakas *et al.* (1999) used the k nearest-neighbour (kNN) algorithm and Landsat TM sensor data to estimate wood volume and biomass on NFI sample plot data. On plot level, Fazakas *et al.* found RMSE higher than (~66 per cent for both forest variables) the ones observed here. Nonetheless, our SRM had a fairly high error rate (Table 2) and a tendency to overestimate in lower-volume forests and underestimate in higher-volume forests (Figure 4), which suggests that the model would need to be enhanced to more accurately estimate the wood volume. It is worth noting that we obtained a better accuracy when the SRMs were modelled by Landsat scene. A single SRM for the whole study area was initially tested and we noted a performance worse than the specific-by-scene SRMs. This supports the approach of fitting the models by scene.

More generally, our review of the literature suggests that are many factors affecting the canopy or vegetation reflectance (Guyot *et al.*, 1989), which in turn affect the accuracy of reflectance-based models, including: geometry of data acquisition, solar illumination, sensor spectral sensibility, canopy format, crown closure, among others. Characteristics of the background vegetation affects the reflectance spectra. For example, infra-red band reflectance values are smaller in vegetation located wet soils (lowland areas) than in dry soils (Adam *et al.*, 2010; Joseph & Jeganathan, 2017). Also, from a same remote sensor, vegetation reflectance spectra change as forest types and sites change. In a study area with different sites, Foody *et al.* (2003) found that the contribution of Landsat bands to predict AGB differed between sites, so that bands that were important at one site were unimportant at other sites. As consequence of this, the vegetation indices that are strongly correlated with AGB also differed between sites, as well as the magnitude and direction of regression parameters. All these facts, therefore, suggest better success with either a single robust model at regional level, or various specific models that capture the variation over large areas. As Brazil contains a wide



diversity of forest types at the national scale, it is of special importance to test stratifications of the NFI plots, when a national database is analyzed. Such strata should aggregate, for example, classes of succession of vegetation, or forest types.

In addition to the issues related to reflectance variations, other sources of error inherent to NFI plots and field collection may have contributed to the loss of accuracy of the SRMs. One of them was the large variation of stand-level volume we observed in NFI plots. We observed entirely forested clusters (i.e. with 40 plots classified into a forest class) with low wood volume, or even without any volume. This situation is typical in ESFs, since the NFI inclusion criteria (of trees with Dbh  $\geq 10$  cm) disregards the smaller trees in young forests. An overstory may have spectral responses similar to a mature forest, given similar 'greenness' and 'wetness' values, for example. However, their forest volume stocks could be much different from each other, portraying a high volume variability over a short reflectance variability.

Incompatibilities between size of NFI's subunits and spatial resolution of sensors may have been another source of error and loss of accuracy, as reported by Fassnacht *et al.* (2014). We observed such problems in our study; the cluster-plot subunits were of 20  $\times$  50 m, so one 30-m pixel exceeds the width of one side of the subunits. This condition obligated us to expand the collection of pixels across the total area covered by the cluster, i.e. 40 000 m<sup>2</sup> (200  $\times$  200 m: North–South/East–West distances = 200 m), instead of collecting only pixels over subunits. Such expansion was performed only in entirely-forested clusters, since the other clusters have non-forest pixels over this area of 40 000 m<sup>2</sup>. In this case, the source of error exists because such expanded area contemplates pixels from non-inventoried parts of the forest, hoping that they have similar stocks to that inventoried ones. If they do not have similar stocks, the underlying pixel reflectances used to calibrate the models may have been incompatible to the ground truth.

As a third source of error, the complex composition and structure from tropical forests (Malhi *et al.*, 1999) also are cited as negative influences to fit satellite-based models (Mallin *et al.*, 2004). Especially in the Brazilian tropical forests, heights of trees is variable over small areas of forest, besides having a high number of tree species. This complexity increases the variation of pixel reflectances, and likely contributed to inaccuracy in the SRMs.

### Performance of the RKM for estimating wood volume at pixel level

Our study revealed that the RKM was able to more finely map forest volumes than the NFI, but this was mainly the result of the fact that it was built on a grid of forested and non-forested pixels and the non-forested areas were clipped from the final coverage (white areas in RK-based mapping in Figure 6). The RKM was unable to accurately estimate forest volumes at specific locations and failed to predict any areas with lesser or greater wood volumes (Figure 5). As a result, RK produced more homogeneous maps of forest volume distribution than SRM (Figure 6). The map based on the SRMs showed a wider range of volumes over the study area, which likely better represents realities observed on the ground. Both methods provided close

estimates for total volume, with relative difference of  $\sim 4$  per cent, which suggests that the RKM captured the mean trend fairly well, but could not effectively spatialize the residuals, with only latitude as a spatial predictor. Wood volume is unlikely to be gradually spatialized in lat./long. gradient, which could hamper the performance of any model based on geographic location. The forested areas tended to follow a similar spatial pattern to the ground slope map (compare Figures 3 and 6). Therefore, in the future, we would recommend using elevation as a third coordinate to possibly improve the RKM estimates.

Our RK method yielded RMSE similar to studies which also used geostatistical methods (Scolforo *et al.*, 2015, 2016; Yadav & Nandy, 2015). Meng *et al.* (2009) tested four geostatistical methods aiming at estimating forest basal area in a region of  $\sim 35\,000$  km<sup>2</sup> and RK provided the smallest errors. The main difference between this study and the one from Meng *et al.* is that they used Landsat ETM+ data as input variables to the linear model, rather than geographical variables. Unlike our RKM, Meng *et al.* showed no limitation in estimating lower or upper values covering the underlying distribution and obtained much better fit statistics for their models (values of  $R^2$  around 0.90). On the other hand, Viana *et al.* (2012) used remotely-sensed data combined with RK for estimating AGB; the authors obtained low performance of the RK method, but they associated this result with a low spatial dependence of the variable. This appears to have been the case in our study.

Aiming to spatialize aboveground carbon (AGC) in tropical forests, Scolforo *et al.* (2016) also used RK combined with longitude, besides another variable related to the biome. The authors obtained an ME of  $\sim 58$  per cent and a residual distribution notably biased, but relatively better than the residuals showed in Figure 4c. A limitation in estimating volume of extreme classes also was noted in Scolforo *et al.*, indicating that their variable of interest (AGC) was limited to longitude, similar to this study, except wood volume was limited to latitude.

In a survey also with AGC, but in a larger study area (State of Minas Gerais, Brazil), Scolforo *et al.* (2015) selected the variables latitude and altitude in the model used to the RK. In this case, their residuals were much less biased than the residuals shown in Figure 4c. The inclusion of altitude in the model, possibly contributed to a better residual distribution. Elevation is commonly related to AGB and carbon, and is thus often used to estimate such variables (Houghton *et al.*, 2001; Zhang *et al.*, 2009; Alves *et al.*, 2010).

### Conclusions

This study explored two methods to extrapolate NFI cluster plot volume estimates, which are currently extrapolated from a 20-km spatial resolution to a very-fine 30-m scale resolution, using a SRM built off 30-m Landsat imagery, or an RKM that uses that coordinates of the centre points of pixels, without using the reflectance values of the pixels. The SRM-based method captured the mean and the general spatial trend in forest volume in a 30-m resolution map, though it did so with a significant bias. The RK-based method also well estimated the mean trend of wood volume, but completely failed to predict any areas with high or low forest volume and was unable to capture a meaningful spatial trend, with spatialized residuals having only

latitude as a weak predictor of volume distribution within the region. The current RKMs need more refinement to eliminate bias and reduce prediction error, before such models could be used operationally.

The SRM produced a higher overall estimate of forest volume for the region than the 'standard' estimate provided by the NFI, with a lower relative error ( $\pm 5$  per cent versus  $\pm 16$  per cent). Combined with other analyses presented here, the results suggest that the NFI cluster plot resolution may be too coarse to be accurately representing the amount forest cover in the region and a remote-sensing-assisted SRM approach could be an effective way enhance predictions from the NFI ground data. Our results also suggest developing multiple SRMs over smaller regions of larger areas might be more effective than using a single SRM to cover a large area.

## Supplementary data

Supplementary data are available at *Forestry* online.

## Conflict of interest statement

None declared.

## References

- Adam, E., Mutanga, O. and Rugege, D. 2010 Multispectral and hyperspectral remote sensing for identification and mapping of wetland vegetation: a review. *Wetl. Ecol. Manag.* **18**, 281–296.
- Alves, L.F., Vieira, S.A., Scaranello, M.A., Camargo, P.B., Santos, F.A.M., Joly, C.A., et al 2010 Forest structure and live aboveground biomass variation along an elevational gradient of tropical Atlantic moist forest (Brazil). *For. Ecol. Manage.* **260**, 679–691.
- Angulo-Martínez, M., López-Vicente, M., Vicente-Serrano, S.M. and Beguería, S. 2009 Mapping rainfall erosivity at a regional scale: a comparison of interpolation methods in the Ebro Basin (NE Spain). *Hydrol. Earth Syst. Sci.* **13**, 1907–1920.
- Bechtold, W. A., Patterson, Paul, L. 2005 *The enhanced forest inventory and analysis program - national sampling design and estimation procedures*. Gen. Tech. Rep. SRS-80. Asheville, NC: U.S. Department of Agriculture, Forest Service, Southern Research Station. 85 p.
- Berk, A., Anderson, G.P., Bernstein, L.S., Acharya, P.K., Dothe, H., Matthew, M.W., et al 1999 'MODTRAN4 radiative transfer modeling for atmospheric correction' Proc. SPIE 3756, Optical Spectroscopic Techniques and Instrumentation for Atmospheric and Space Research III.
- Berra, E.B., Brandelero, C., Pereira, R.S., Sebem, E., Goergen, L.C.G., Benedetti, A.C.P., et al 2012 Estimativa do volume total de madeira em espécies de eucalipto a partir de imagens de satélite Landsat. *Ciência Florestal* **22**, 853–864.
- Blaschke, T. 2010 Object based image analysis for remote sensing. *ISPRS J. Photogramm. Remote Sens.* **65**, 2–16.
- Bohlin, J., Bohlin, I., Jonzén, J. and Nilsson, M. 2017 Mapping forest attributes using data from stereophotogrammetry of aerial images and field data from the national forest inventory. *Silva Fennica* **51**, 1–18.
- Brasil. 1994 CONAMA - Conselho Nacional Do Meio Ambiente. Resolução nº 2, de 18 de Março de 1994. Diário Oficial da República Federativa do Brasil, Brasília, DF.
- Brooks, E.B., Coulston, J.R., Wynne, R.H. and Thomas, A. 2016 Improving the precision of dynamic forest parameter estimates using Landsat. *Remote Sens. Environ.* **179**, 162–169.
- Cambardella, C.A., Moorman, T.B., Novak, J.M., Parkin, T.B., Karlen, D.L., Turco, R.F., et al 1994 Field-scale variability of soil properties in central Iowa soils. *Soil Sci. Soc. Am. J.* **58**, 1501–1511.
- Chacko, J. 1965 *A manual on sampling techniques for forest surveys*. India, P.Z.O., p. 172.
- Cohen, W.C. and Goward, S.N. 2004 Landsat's role in ecological applications of remote sensing. *Bioscience* **54**, 535–545.
- Congalton, R.G. and Green, K. 2008 *Assessing the Accuracy of Remotely Sensed Data: Principles and Practices*. 2nd edn. CRC Press.
- David, H.C. 2018. Estimating and mapping forest variables of the Brazilian National Forest Inventory to finer scales. Thesis (PhD in Forest Management). Universidade Federal do Paraná, Curitiba, Brazil. 116p.
- David, H.C., Araújo, E.J.G., Morais, A., Scolforo, J.R.S., Marques, J.M., Pellico Netto, S., et al 2017 Carbon stock classification for tropical forests in Brazil: understanding the effect of stand and climate variables. *For. Ecol. Manage.* **404**, 241–250.
- Deo, R.K., Russell, M.B., Domke, G.M., Woodall, C.W., Falkowski, M.J. and Cohen, W.B. 2017 Using landsat time-series and LiDAR to inform above-ground forest biomass baselines in Northern Minnesota, USA. *Can. J. Remote Sens.* **43**, 28–47.
- Dube, T. and Mutanga, O. 2015 Evaluating the utility of the medium-spatial resolution Landsat 8 multispectral sensor in quantifying above-ground biomass in uMgeni catchment, South Africa. *ISPRS J. Photogramm. Remote Sens.* **101**, 36–46.
- Fassnacht, F.E., Hartig, F., Latifi, H., Berger, C., Hernández, J., Corvalán, P., et al 2014 Importance of sample size, data type and prediction method for remote sensing-based estimations of aboveground forest biomass. *Remote Sens. Environ.* **154**, 102–114.
- Fazakas, Z., Nilsson, M. and Olsson, H. 1999 Regional forest biomass and wood volume estimation using satellite data and ancillary data. *Agric. For. Meteorol.* **98–99**, 417–425.
- Finley, A.O., Banerjee, S. and MacFarlane, D.W. 2011 A hierarchical model for quantifying forest variables over large heterogeneous landscapes with uncertain forest areas. *J. Am. Stat. Assoc.* **106**, 31–48.
- Foody, G.M., Boyd, D.S. and Cutler, M.E.J. 2003 Predictive relations of tropical forest biomass from Landsat TM data and their transferability between regions. *Remote Sens. Environ.* **85**, 463–474.
- Franklin, S.E. 2001 *Remote sensing for sustainable forest management*. Lewis Publishers, p. 407.
- Freitas, J., de Oliveira, Y.M., Rosot, M.A., Gomide, G. and Mattos, P.P. 2010 Chapter 3. Brazil. In *National forest inventories: Pathways for common reporting*. Tomppo E., Gschwanter T., Lawrence M. and McRoberts R.E. (eds). Springer, p. 612.
- Gleason, C.J. and Im, J. 2011 A review of remote sensing of forest biomass and biofuel: options for small-area applications. *GISci. Remote Sens.* **48**, 141–170.
- Gobakken, T., Naesset, E., Nelson, R., Bollandsas, O.M., Gregoire, T.G., Stahl, G., et al 2012 Estimating biomass in Hedmark County, Norway using national forest inventory field plots and airborne laser scanning. *Remote Sens. Environ.* **123**, 443–456.
- Guyot, G., Guyon, D. and Riom, J. 1989 Factors affecting the spectral response of forest canopies: a review. *Geocarto Int.* **4**, 3–18.
- Hall, R.J., Skakun, R.S., Arsenault, R.J. and Case, B.S. 2006 Modeling forest stand structure attributes using Landsat ETM+ data: application to mapping of aboveground biomass and stand volume. *For. Ecol. Manage.* **225**, 378–390.
- Hayashi, R., Kershaw, J.A., Jr. and Weiskittel, A. 2015 Evaluation of alternative methods for using LIDAR to predict aboveground biomass in

- mixed species and structurally complex forests in Northeastern North America. *Math. Comput. For. Nat. Res. Sci* **7**, 49–65.
- Houghton, R.A., Lawrence, K.T., Hackler, J.L. and Brown, S. 2001 The spatial distribution of forest biomass in the Brazilian Amazon: a comparison of estimates. *Glob. Change Biol.* **7**, 731–746.
- Johnson, R.A. and Wichern, D.W. 2007 *Applied Multivariate Statistical Analysis*. 5th edn. Pearson Prentice Hall, p. 808.
- Joseph, G. and Jeganathan, C. 2017 *Fundamentals of Remote Sensing*. 3rd edn. Universities Press, p. 624.
- Kachhwaha, T.S. 1983 Spectral signatures obtained from Landsat data for forest vegetation and land-use mapping in India. *Photogramm. Eng. Remote Sens.* **49**, 685–689.
- Kim, H., Bettinger, P. and Cieszewski, C. 2013 Reflections on the estimation of stand-level forest characteristics using landsat satellite imagery. *Appl. Remote Sens. J.* **2**, 45–56.
- Krankina, O.N., Harmon, M.E., Cohen, W.B., Oetter, D.R., Zyrina, O. and Duane, M.V. 2004 Carbon stores, sinks, and sources in forests of Northwestern Russia: can we reconcile forest inventories with remote sensing results? *Clim. Change* **67**, 257–472.
- Labrecque, S., Fournier, R.A., Luther, J.E. and Piercey, D. 2006 A comparison of four methods to map biomass from Landsat-TM and inventory data in western Newfoundland. *For. Ecol. Manage.* **226**, 129–144.
- Landis, J. and Koch, G. 1977 The measurement of observer agreement for categorical data. *Biometrics* **33**, 159–174.
- Lu, D., Chen, Q., Wang, G., Moran, E., Batistella, M., Zhang, M., et al 2012 Aboveground forest biomass estimation with landsat and LiDAR data and uncertainty analysis of the estimates. *Int. J. For. Res.* **2012**, 1–16.
- Lu, D., Mausel, P., Brondizio, E. and Moran, E. 2004 Relationships between forest stand parameters and Landsat TM spectral responses in the Brazilian Amazon Basin. *For. Ecol. Manage.* **198**, 149–167.
- Maack, J., Lingenfelder, M., Weinacker, H. and Koch, B. 2016 Modelling the standing timber volume of Baden-Württemberg—a large-scale approach using a fusion of Landsat, airborne LiDAR and National Forest Inventory data. *Int. J. Appl. Earth Obs. Geoinf.* **49**, 107–116.
- Mäkelä, H. and Pekkarinen, A. 2004 Estimation of forest stand volumes by Landsat TM imagery and stand-level field-inventory data. *For. Ecol. Manage.* **196**, 245–255.
- Malhi, Y., Baldocchi, D.D. and Jarvis, G. 1999 The carbon balance of tropical, temperate and boreal forests. *Plant Cell Environ.* **22**, 715–740.
- Mallinis, G., Koutsias, N., Makras, A. and Karteris, M. 2004 Forest parameters estimation in a European Mediterranean landscape using remotely sensed data. *For. Sci.* **50**, 450–460.
- McRoberts, R.E., Liknes, G.C. and Domke, G.M. 2014 Using a remote sensing-based, percent tree cover map to enhance forest inventory estimation. *For. Ecol. Manage.* **331**, 12–18.
- McRoberts, R.E., Moser, P., Oliveira, L.Z. and Vibrans, A.C. 2015 A general method for assessing the effects of uncertainty in individual-tree volume model predictions on large-area volume estimates with a subtropical forest illustration. *Can. J. For. Res.* **45**, 44–51.
- McRoberts, R.E. and Tomppo, E.O. 2007 Remote sensing support for national forest inventories. *Remote Sens. Environ.* **110**, 412–419.
- Mello, C.R., Viola, M.R., Owens, R., Mello, J.M. and Beskow, S. 2015 Interpolation methods for improving the RUSLE R-factor mapping in Brazil. *J. Soil Water Conserv.* **70**, 182–197.
- Meng, Q., Cieszewski, C. and Madden, M. 2009 Large area forest inventory using Landsat ETM+: a geostatistical approach. *ISPRS J. Photogramm. Remote Sens.* **64**, 27–36.
- Mohammadi, J., Joibary, S.S., Yaghmaee, F. and Mahiny, A.S. 2010 Modelling forest stand volume and tree density using Landsat ETM+ data. *Int. J. Remote Sens.* **31**, 2959–2975.
- Nazeer, M., Nichol, J.E. and Yung, Y.-K. 2014 Evaluation of atmospheric correction models and Landsat surface reflectance product in an urban coastal environment. *Int. J. Remote Sens.* **35**, 1–21.
- Odeh, I.O.A., Mcbratney, A.B. and Chittleborough, D.J. 1995 Further results on prediction of soil properties from terrain attributes: heterotopic cokriging and regression-kriging. *Geoderma* **67**, 215–226.
- Powell, S.L., Cohen, W.B., Healey, S.P., Kennedy, R.E., Moisen, G.G., Pierce, K. B., et al 2010 Quantification of live aboveground forest biomass dynamics with Landsat time-series and field inventory data: a comparison of empirical modeling approaches. *Remote Sens. Environ.* **114**, 1053–1068.
- Ribeiro Junior, J. and Diggle, J. 2001 geoR: a package for geostatistical analysis. *R-NEWS* **1**, 15–18.
- Scolforo, H.F., Scolforo, J.R.S., Mello, C.R., Mello, J.M. and Ferraz Filho, A.C. 2015 Spatial distribution of aboveground carbon stock of the arboreal vegetation in Brazilian Biomes of Savanna, Atlantic Forest and Semi-Arid Woodland. *PLoS One* **10**, 1–20.
- Scolforo, H.F., Scolforo, J.R.S., Mello, J.M., Mello, C.R. and Morais, A. 2016 Spatial interpolators for improving the mapping of carbon stock of the arboreal vegetation in Brazilian biomes of Atlantic forest and Savanna. *For. Ecol. Manage.* **376**, 24–35.
- Tomppo, E., Nilsson, M., Rosengren, M., Aalto, P. and Kennedy, P. 2002 Simultaneous use of Landsat-TM and IRS-1C WiFS data in estimating large area tree stem volume and aboveground biomass. *Remote Sens. Environ.* **82**, 156–171.
- Tomppo, E., Olsson, H., Ståhl, G., Nilsson, M., Hagner, O. and Katila, M. 2008 Combining national forest inventory field plots and remote sensing data for forest databases. *Remote Sens. Environ.* **112**, 1982–1999.
- Trimble. 2011. eCognition Developer 8.64.1 User Guide. Munich: Trimble Germany.
- Trishchenko, A.P., Cihlar, J. and Li, Z. 2002 Effects of spectral response function on surface reflectance and NDVI measured with moderate resolution satellite sensors. *Remote Sens. Environ.* **81**, 1–18.
- Viana, H., Lopes, A. D., Cohen, W. B. 2012 Estimation of crown biomass of *Pinus pinaster* stands and shrubland above-ground biomass using forest inventory data, remotely sensed imagery and spatial prediction models. *Ecol. Modell.* **226**, 22–35.
- Vibrans, A. C., McRoberts, R. E., Moser, P., Nicoletti, A. L. 2013 Using satellite image-based maps and ground inventory data to estimate the area of the remaining Atlantic forest in the Brazilian state of Santa Catarina. *Remote Sens. Environ.* **130**, 87–95.
- Wackernagel, H. 2003 *Multivariate Geostatistics: An Introduction with Applications*. 3rd edn. Springer-Verlag Berlin Heidelberg, p. 388.
- Weber, E., Hasenack, H. and Ferreira, C.J.S. 2004 Adaptação do modelo digital de elevação do SRTM para o sistema de referência oficial brasileiro e recorte por unidade da federação. Porto Alegre, UFRGS: Centro de Ecologia.
- Wilson, B.T., Woodall, C.W. and Griffith, D.M. 2013 Imputing forest carbon stock estimates from inventory plots to a nationally continuous coverage. *Carbon Balance Manag.* **8**, 1–15.
- Yadav, K.V. and Nandy, S. 2015 Mapping aboveground woody biomass using forest inventory, remote sensing and geostatistical techniques. *Environ. Monit. Assess.* **187**, 1–12.
- Zhang, X., Wang, M. and Liang, X. 2009 Quantitative classification and carbon density of the forest vegetation in Lüliang Mountains of China. *Plant Ecol.* **201**, 1–9.